J. Wind Eng. Ind. Aerodyn. 99 (2011) 267–278

Contents lists available at ScienceDirect

Journal of Wind Engineering and Industrial Aerodynamics

journal homepage: www.elsevier.com/locate/jweia

Improved k–ε model and wall function formulation for the RANS simulation of ABL flows

A. Parente [a,b,*], C. Gorlé [c], J. van Beeck [a], C. Benocci [a]

[a] Environmental and Applied Fluid Dynamic Department, Von Karman Institute for Fluid Dynamics, Bruxelles, Belgium
[b] Service d'Aéro-Thermo-Mécanique, Université Libre de Bruxelles, Bruxelles, Belgium
[c] Center for Turbulence Research, Stanford University, Stanford, CA, USA

ARTICLE INFO

Available online 4 February 2011

Keywords:
ABL
Rough wall function
Turbulent kinetic energy
k-Epsilon turbulence model
RANS

ABSTRACT

The simulation of Atmospheric Boundary Layer (ABL) flows is usually performed using the commercial CFD codes with RANS turbulence modelling and standard sand–grain rough wall functions. Such approach generally results in the undesired decay of the velocity and turbulent profiles specified at the domain inlet, before they reach the section of interest within the computational domain. This behaviour is a direct consequence of the inconsistency between the fully developed ABL inlet profiles and the wall function formulation.

The present paper addresses the aforementioned issue and proposes a solution to it. A modified formulation of the Richards and Hoxey wall function for turbulence production is presented to avoid the well-documented over-prediction of the turbulent kinetic energy at the wall. Moreover, a modification of the standard k–ε turbulence model is proposed to allow specific arbitrary sets of fully developed profiles at the inlet section of the computational domain.

The methodology is implemented and tested in the commercial code FLUENT v6.3 by means of the User Defined Functions (UDF). Results are presented for two neutral boundary layers over flat terrain, at wind tunnel and full scale, and for the flow around a bluff-body immersed into a wind-tunnel ABL. The potential of the proposed methodology in ensuring the homogeneity of velocity and turbulence quantities throughout the computational domain is demonstrated.

1. Introduction

The limitations related to the Reynolds-averaged Navier–Stokes (RANS) simulation of the neutral atmospheric boundary layer (ABL) with the commercial CFD codes are well known and documented in the literature (Franke et al., 2007; Blocken et al., 2007a, b; Riddle et al., 2004; Hargreaves and Wright, 2007). The cause of such unsatisfactory behaviour is directly related to inconsistencies between the formulation of the law of the wall for rough surfaces and the inlet conditions for the ABL simulations. Remedial measures have been proposed in the literature (Blocken et al., 2007b); however, these are generally code-dependant and do not provide a general solution to the problem. In particular, the effect of roughness on turbulent quantities is not explicitly taken into account, causing an undesired non-homogeneity of the turbulent quantities throughout the computational domain.

As far as inlet profiles for the ABL simulations are concerned, fully developed profiles by Richards and Hoxey (1993) are usually used as inlet conditions. However, the assumption of constant kinetic energy, k, is not consistent with wind-tunnel measurements (Leitl, 1998; Xie et al., 2004; Yang et al., 2009), where a variation of k with height is generally observed. Following these considerations, Yang et al. (2009) proposed a new set of inlet conditions, where the k profile is a function of height; however, the consistency between this new set of inlet conditions and the k–ε model equations was not completely tackled. In a recent work, Gorlé et al. (2009) proposed formulations for the C_μ and σ_ε turbulence model constants to ensure stream-wise homogeneity when using the k profile proposed by Yang et al. (2009).

In case of full-scale ABL applications, semi-empirical correlations are provided to estimate the level of turbulent kinetic energy, based on the ABL friction velocity and height (Brost and Wyngaard, 1978). However, modifications need to be brought to the turbulence model, to ensure that the resulting set of fully developed profiles satisfies the transport equations.

The objective of the present paper is to develop an improved k–ε turbulence model for the numerical simulation of neutral ABL flows, with arbitrary sets of fully developed inlet conditions. This is

* Corresponding author at: Service d'Aéro-Thermo-Mécanique, Université Libre de Bruxelles, Bruxelles, Belgium. Tel.: +3226502680; fax: +3226502710.
E-mail address: Alessandro.Parente@ulb.ac.be (A. Parente).

0167-6105/$ - see front matter © 2011 Elsevier Ltd. All rights reserved.
doi:10.1016/j.jweia.2010.12.017

accomplished through the introduction of two source terms in the transport equations of k and ε, to ensure that the profiles identically satisfy the ABL model equations. Moreover, the overall consistency of the approach is ensured through a novel implementation of a general-purpose wall function for rough surfaces, based on the aerodynamic roughness, as indicated by Richards and Hoxey (1993).

2. Theory

The equations describing a 2-dimensional ABL with the standard k–ε model, under the hypothesis of (i) zero vertical velocity, (ii) constant pressure along vertical and stream-wise directions and (iii) constant shear stress, reduce to:

$$\mu_T \frac{\partial u}{\partial z} = \tau_w = \rho u^{*2} \tag{1}$$

$$\frac{\partial}{\partial z}\left(\frac{\mu_t}{\sigma_k}\frac{\partial k}{\partial z}\right) + G_k - \rho\varepsilon = 0 \tag{2}$$

$$\frac{\partial}{\partial z}\left(\frac{\mu_t}{\sigma_\varepsilon}\frac{\partial \varepsilon}{\partial z}\right) + C_{\varepsilon 1} G_k \frac{\varepsilon}{k} - C_{\varepsilon 2}\rho\frac{\varepsilon^2}{k} = 0 \tag{3}$$

where the dynamic viscosity has been neglected with respect to the turbulent viscosity ($\mu_t \gg \mu$). The production of turbulent kinetic energy, G_k, and the turbulent viscosity, μ_t, are given by

$$G_k = \mu_t\left(\frac{\partial u}{\partial z}\right)^2, \quad \mu_t = \rho C_\mu \frac{k^2}{\varepsilon} \tag{4}$$

and σ_k, σ_ε, $C_{\varepsilon 1}$, $C_{\varepsilon 2}$ and C_μ are constants of the k–ε turbulence model.

To correctly simulate a fully developed ABL, the velocity, turbulent kinetic energy and turbulent dissipation rate profiles specified at the inlet boundary should satisfy Eqs. (1)–(3). The consistency between fully developed inlet boundary conditions and turbulence model formulation is discussed in Section 2.1. In addition, it should be guaranteed that the boundary condition applied at the wall correctly represents the influence of the surface roughness. This topic is discussed in Section 2.2.

2.1. Improved k–ε turbulence model formulation

In the framework of ABL simulations, fully developed inlet profiles for velocity and turbulent quantities are generally prescribed at the inlet section of the computational domain. Mathematically, this implies that these profiles identically satisfy Eqs. (1)–(3).

Richards and Hoxey (1993) proposed profiles of mean velocity, turbulent kinetic energy and dissipation rate for neutral stratification conditions:

$$u = \frac{u^*}{\kappa}\ln\left(\frac{z+z_0}{z_0}\right) \tag{5}$$

$$k = \frac{u^{*2}}{\sqrt{C_\mu}} \tag{6}$$

$$\varepsilon = \frac{u^{*3}}{\kappa(z+z_0)} \tag{7}$$

It can be shown that Eqs. (5)–(7) are analytical solutions of the momentum and k–ε model equations if the turbulent dissipation number Prandtl number is given by

$$\sigma_\varepsilon = \frac{\kappa^2}{(C_{\varepsilon 2} - C_{\varepsilon 1})\sqrt{C_\mu}} \tag{8}$$

The condition expressed by Eq. (8) is obtained by substituting the imposed profiles of turbulent kinetic energy and dissipation rate in the transport equation for ε and solving for σ_ε. Alternatively, the constant value of σ_ε can be maintained and a source term added to the dissipation rate equation:

$$S_\varepsilon(z) = \frac{\rho u^{*4}}{(z+z_0)^2}\left(\frac{(C_2 - C_1)\sqrt{C_\mu}}{\kappa^2} - \frac{1}{\sigma_\varepsilon}\right) \tag{9}$$

A similar approach was adopted by Pontiggia et al. (2009) who retained, however, the molecular viscosity in their derivation. Different from Eq. (8), the introduction of a source term in the transport equation for ε does not require the calculation of σ_ε for each computation as S_ε self-adapts to the characteristics of the ABL under investigation.

The fully developed profiles provided by Richards and Hoxey (1993) are mathematically consistent, i.e. they are a solution of the mathematical models describing a homogeneous ABL. However, the choice of a constant k profile (Eq. (6)) contradicts the experimental evidence showing a trend in decreasing k with height (Leitl, 1998; Xie et al., 2004; Yang et al., 2009). Recently, Yang et al. (2009) analytically derived an inlet condition for turbulent kinetic energy as a function of the height from the ground:

$$k(z) = \sqrt{C_1 \ln(z+z_0) + C_2} \tag{10}$$

where C_1 and C_2 are constants that can be determined by fitting the measured profile of k. By assuming equilibrium between turbulent production and dissipation, the turbulent dissipation rate profile can be expressed as

$$\varepsilon(z) = \sqrt{C_\mu} k \frac{du}{dz} \tag{11}$$

As far as the consistency between fully developed inlet conditions and turbulence model is concerned, Yang et al. (2009) argued that the profile expressed by Eq. (10) identically satisfies the transport equation for k. However, they did not take into account the implications of a non-constant k profile on the momentum and turbulent dissipation rate transport equation. In particular, a general condition on the turbulence model parameter C_μ can be deduced substituting Eq. (11) into Eq. (1) and employing the definition of turbulent viscosity (Eq. (4)):

$$C_\mu(z) = \frac{u^{*4}}{k(z)^2} \tag{12}$$

Eq. (12) is simply the relation proposed by Richards and Hoxey (1993) inverted, to ensure consistency between the turbulence model, i.e. C_μ, and the k profile throughout the ABL domain. From the point of view of the physical interpretation, the non-uniform k profile and the definition of C_μ can be related to the large-scale turbulence present in the ABL flows, which can vary significantly with height. Bottema (1997) indicated the relevance of large-scale turbulence to several RANS models, pointing out the necessity for case- and location-dependant model constants. The present paper follows this approach proving a model defining optimal local values of C_μ, according to Eq. (12). It is also noted that the assumption of equilibrium between production and dissipation, which results in the proposed relation for C_μ, implies that the gradient of turbulent kinetic energy does not introduce vertical diffusion of k. This assumption was justified by estimating the magnitude of the diffusion term based on the experimental data, which resulted negligible compared to the production of turbulence kinetic energy.

In addition to specifying C_μ according to Eq. (12), a source term is added to the transport equation of turbulent kinetic energy, to ensure equilibrium between production and dissipation. This is due to the fact that for a non-uniform C_μ, the analytic profile derived by Yang et al. (2009) is no longer a solution of the k transport equation and the following extra term appears when

substituting Eqs. (10)–(12) in Eq. (2):

$$S_k(z) = \frac{\rho u^* \kappa}{\sigma_k} \frac{\partial}{\partial z}\left((z+z_0)\frac{\partial k}{\partial z}\right) \tag{13}$$

This formulation of the source term is valid for any shape of the k inlet profile, as long as the k gradient in the vertical direction is specified.

As far as the transport equation for ε is concerned, Eq. (8) for σ_ε or, alternatively, Eq. (9) for S_ε is still valid. This is a consequence of the equilibrium assumption and of the generalisation of C_μ (Eq. (12)), which makes the first term of the ε transport equation independent of the form of the specified inlet profile:

$$\frac{\partial}{\partial z}\left(\frac{\mu_t}{\sigma_\varepsilon}\frac{\partial \varepsilon}{\partial z}\right) = \frac{\rho u^{*4}}{\sigma_\varepsilon (z+z_0)^2} \tag{14}$$

In summary, a consistent formulation of the inlet conditions and the k–ε turbulence model is obtained when specifying Eq. (5) for u, a freely chosen profile for k (e.g. Eq. (6) or Eq. (10)), Eq. (11) for ε and adding the source terms from Eq. (13) and Eq. (9) to the transport equations for k and ε, respectively.

The profile proposed by Yang et al. (2009) requires the availability of experimental data to determine the parameters C_1 and C_2 of Eq. (10). This is not always guaranteed, especially for full-scale measurements. In this case, semi-empirical parameterizations available in the literature can be applied for the turbulent quantities. Brost and Wyngaard (1978) provided the following expressions for the mean squared fluctuating velocity components:

$$\frac{\langle u'^2\rangle}{u^{*2}} = 5-4\frac{z}{h}; \quad \frac{\langle v'^2\rangle}{u^{*2}} = 2-\frac{z}{h}; \quad \frac{\langle w'^2\rangle}{u^{*2}} = 1.7-\frac{z}{h} \tag{15}$$

where h represents the ABL height. For neutral stratification conditions the value of h can be deduced from the following relation (Bechmann, 2006):

$$\frac{h f_c}{u^{*2}} \approx 0.33 \tag{16}$$

where a typical mid-latitude value for the Coriolis parameter, $f_c = 10^{-4}$, was chosen. The variation of turbulent kinetic energy with height can be then expressed as

$$k(z) = \frac{1}{2}(\langle u'^2\rangle + \langle v'^2\rangle + \langle w'^2\rangle) = \frac{u^{*2}}{2}\left(8.7-6\frac{z}{h}\right) \tag{17}$$

As stated earlier, the use of a specific inlet profile for k does not affect the formulation of the turbulence model. As long as the profile for ε is specified according to Eq. (11), the source terms for turbulent kinetic energy and dissipation rate (Eqs. (9) and (13)) ensure that the set of inlet conditions is consistent with the turbulence model formulation.

2.2. Novel rough wall function formulation

In the CFD software, rough surfaces are generally modelled with an extension of the standard smooth law of the wall:

$$\frac{u}{u^*} = \frac{1}{\kappa}\ln(Ez^+) - \Delta B(k_s^+) \tag{18}$$

where u^* is the friction velocity, κ is the Von Karman constant, E is an integration constant and z^+ is the non-dimensional distance from the wall, defined as $z^+ = zu^*/\nu$. The function ΔB depends on the dimensionless roughness height $k_s^+ = k_s u^*/\nu$ and quantifies the departure of the wall velocity from smooth conditions. It can assume different forms, depending on the equivalent sand–grain roughness values (Cebeci and Bradshaw, 1977; Nikuradse, 1933). In particular, when $k_s^+ > 90$, Eq. (16) can be reformulated as

$$\frac{u}{u^*} \approx \frac{1}{\kappa}\ln\left(\frac{Ez^+}{C_s k_s^+}\right) \tag{19}$$

where C_s is a roughness constant, which should be set to ensure first order matching between the law of the wall and the inlet profile (Blocken et al., 2007b)

$$C_s = \frac{Ez_0}{k_s} = \frac{Ez_0}{z_p} \tag{20}$$

In Eq. (20), a common requirement of the ABL simulations has been made explicit, namely that the distance z_p between the centroid of the wall-adjacent cell and the wall should be larger than the sand-equivalent roughness k_s of the terrain. This requirement is generally translated into an upper limit for k_s, taken equal to z_p.

Different implementations of Eq. (19) can be found in the commercial CFD codes. Currently, the value of C_s can be freely set in the commercial software StarCCM+ (CD-Adapco, 2008). In Ansys CFX, a fixed value for the roughness constant is adopted, $C_s = 0.3$ (Ansys Ltd., 2005), whereas FLUENT (Fluent, 2006) allows defining custom profiles for C_s through user defined functions (UDF).

However, even when Eq. (18) is satisfied, the standard rough wall function suffers from two main drawbacks.

First, it poses strong limitations on the maximum size of the wall-adjacent cell, the maximum allowable value for C_s being limited by the wall function constant E. At the first cell centroid, z_p, Eqs. (19) and (20) give:

$$\frac{u}{u^*} \approx \frac{1}{\kappa}\ln\left(\frac{E}{C_s}\right) \tag{21}$$

assuming $k_s = z_p$. This implies that C_s cannot be higher than the value of the parameter E.

Moreover, the standard wall function does not imply any direct effect of the roughness properties on the turbulence quantities at the wall. To overcome these drawbacks, the Richards and Hoxey (1993) boundary condition has been implemented at the wall to specify velocity, turbulent kinetic energy and turbulent dissipation rate consistently with the inlet profiles and turbulence model:

$$u_w = \frac{u^*}{\kappa}\ln\left(\frac{z_p+z_0}{z_0}\right) \tag{22}$$

$$\varepsilon_w = \frac{C_\mu^{0.75} k^{1.5}}{\kappa(z_p+z_0)} \tag{23}$$

$$G_k = \frac{\tau_w^2}{\rho\kappa C_\mu^{0.25} k^{0.5}(z_p+z_0)} \tag{24}$$

Different from Richards and Hoxey (1993), the production of turbulent kinetic energy at the wall is not integrated over the first cell height, i.e. $\overline{G}_k = 1/(2z_p)\int_0^{2z_p} G_k\,dz$, but computed at the first cell centroid. This formulation is preferred as it is found not to produce the peak of turbulent kinetic energy at the wall observed by Richards and Hoxey (1993) and Hargreaves and Wright (2007). Fig. 1 shows the turbulent kinetic energy at the inlet and outlet sections of an empty domain, where fully developed profiles of velocity and turbulence are specified at the domain inlet according to Eqs. (5)–(7). The test case will be described in detail in Section 3.2. At this point, Fig. 1 is presented to show how the proposed wall function formulation (green dots) provides the best agreement (deviation below 4%) between the profile specified at the inlet and the one retrieved at the outlet. By averaging both G_k and ε (blue short-dashes), the deviation at the wall is about 15%, but it remains higher than the error obtained using the cell values of G_k and ε. Averaging G_k over the first cell, while keeping the cell value for ε (red dashes), leads to an overestimation of the turbulent kinetic energy at the wall of about 100%. Norris and Richards (2010) have shown that such a peak in the profile for k can also be avoided by changing the discretization of the production term, to ensure equilibrium between production and dissipation.

As far as the numerical implementation is concerned, the form of the universal law of the wall is preserved, i.e. $u = u^*/\kappa \ln(E' z^{+\prime})$, through the introduction of a new wall function constant and non-dimensional wall distance, defined as (Parente and Benocci, 2010)

$$E' = \frac{\nu}{z_0 u^*}, \quad z^{+\prime} = \frac{(z+z_0)u^*}{\nu} \tag{25}$$

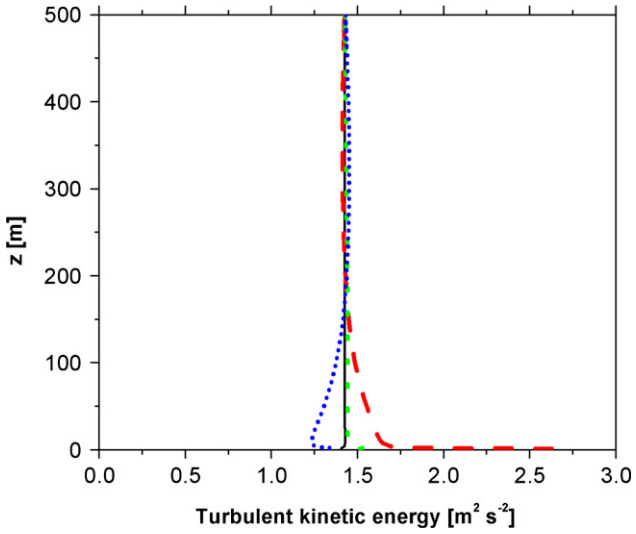

Fig. 1. Turbulent kinetic energy profiles at the inlet and outlet sections of the computational domain (see Fig. 2b). Dashes: cell value for turbulent dissipation rate and turbulent kinetic energy averaged over the first cell. Short dashes: cell value for turbulent dissipation rate and kinetic energy. Dots: turbulent dissipation rate and kinetic energy averaged over the first cell. (For interpretation of the references to colour in this figure, the reader is referred to the web version of this article.)

The non-dimensional distance $z^{+\prime}$ is simply a z^+ shifted by the aerodynamic roughness, whereas the new wall function constant depends on the roughness characteristics of the surface. In Eq. (25) the friction velocity, u^*, is not kept constant in the longitudinal direction but calculated locally as $u^* = C_\mu^{0.25} k_p^{0.5}$.

The present approach removes the drawbacks of the standard wall function, without limiting its flexibility. In particular, it is easily extendable to mixed rough and smooth surface through a redefinition of the law of the wall constants. Moreover, it allows full flexibility from the point of view of mesh generation, as the wall function parameters do not impose any limitation on the first cell height.

3. Test cases

The first step towards the validation of the proposed approach is to prove that it produces sustainable ABL profiles of velocity and turbulence. In other words, the first objective of the present work is to demonstrate that the fully developed inlet profiles imposed at the inlet section of the domain are maintained throughout an empty domain.

Then, the flow around a single, rectangular building is simulated, to investigate the potential of the model in more complex configurations, characterised by the presence of rough and smooth surfaces and separated regions.

3.1. Wind-tunnel unperturbed ABL

The first test case is a wind-tunnel scale ABL (Leitl, 1998), fully characterised in terms of velocity and turbulence intensity measurements. Results are presented for a 2D domain of 4 m length and 1 m height, with a grid of 400 × 71 cells. The domain (Fig. 2a)

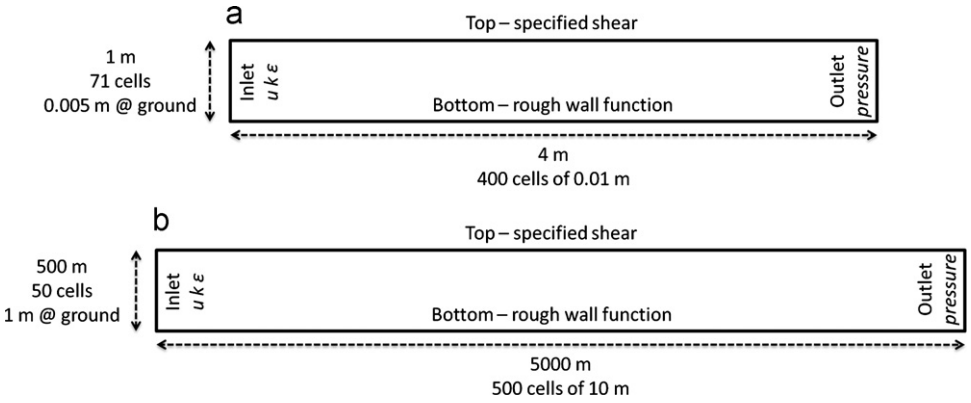

Fig. 2. Computational domain and main boundary conditions applied for the numerical simulation of the unperturbed ABL at wind tunnel (a) and full (b) scale.

Table 1
Summary of the investigated runs and model settings. BIA=Building influence area; STDWF=Standard WallFunction; MODWF=Modified WallFunction.

Test cases	*k profile*	*WF*	*Outside BIA*			*Inside BIA*		
			C_μ	S_k	S_ε	C_μ	S_ε	S_k
Unperturbed ABL wind tunnel	$\frac{u^{*2}}{\sqrt{C_\mu}}$	STD $C_s = \frac{Ez_0}{z_p}$	0.09	0	$\frac{\rho u^{*4}}{(z+z_0)^2}\left(\frac{(C_2-C_1)\sqrt{C_\mu}}{\kappa^2}-\frac{1}{\sigma_\varepsilon}\right)$	–	–	–
	$\sqrt{C_1 \ln(z+z_0)+C_2}$	MOD	$C_\mu = \frac{u_*^4}{k^2}$	$\frac{\rho u^* \kappa}{\sigma_k}\frac{\partial}{\partial z}\left((z+z_0)\frac{\partial k}{\partial z}\right)$	$\frac{\rho u^{*4}}{(z+z_0)^2}\left(\frac{(C_2-C_1)\sqrt{C_\mu}}{\kappa^2}-\frac{1}{\sigma_\varepsilon}\right)$	–	–	–
Unperturbed ABL full scale	$\frac{\langle u'^2\rangle+\langle v'^2\rangle+\langle w'^2\rangle}{2}$	MOD	$C_\mu = \frac{u_*^4}{k^2}$	$\frac{\rho u^* \kappa}{\sigma_k}\frac{\partial}{\partial z}\left((z+z_0)\frac{\partial k}{\partial z}\right)$	$\frac{\rho u^{*4}}{(z+z_0)^2}\left(\frac{(C_2-C_1)\sqrt{C_\mu}}{\kappa^2}-\frac{1}{\sigma_\varepsilon}\right)$	–	–	–
Flow around a bluff-body	$\sqrt{C_1 \ln(z+z_0)+C_2}$	MOD	$C_\mu = \frac{u_*^4}{k^2}$	$\frac{\rho u^* \kappa}{\sigma_k}\frac{\partial}{\partial z}\left((z+z_0)\frac{\partial k}{\partial z}\right)$	$\frac{\rho u^{*4}}{(z+z_0)^2}\left(\frac{(C_2-C_1)\sqrt{C_\mu}}{\kappa^2}-\frac{1}{\sigma_\varepsilon}\right)$	0.09	0	0

is discretized with a grid uniform in the longitudinal direction and stretched in the vertical one to have the centre point of the wall-adjacent cell at a height of 0.0025 m.

At the inlet boundary profiles of velocity, turbulent kinetic energy and dissipation rate are specified. Both the inlet conditions proposed by Richards and Hoxey (1993) and Yang et al. (2009) are tested for turbulent kinetic energy, and the turbulence model parameters are modified accordingly. The values of the ABL parameters used in Eqs. (5) and (10) are $u^*=0.374$ m/s, $z_0=0.00075$ m, $C_1=-0.11$ and $C_2=0.53$.

A pressure outlet condition is applied for the outlet section. Both standard and modified formulations (Section 2.2) for the wall function are applied at the lower boundary, whereas a constant stress is applied to the upper boundary, following the recommendation of Richards and Hoxey (1993). The investigated conditions and model settings are summarised in Table 1.

3.2. Full-scale unperturbed ABL

The second test case is the full-scale ABL adopted for the blind-test exercise on the CFD modelling of wind loading on the full-scale Silsoe cube (Richards et al., 2002). As a prerequisite, the participants were asked to demonstrate that they were able to model a sustainable ABL. Results are presented for a 2D domain (Fig. 2b) of 5000 m length and 500 m height, with a grid of 500×50 cells. The generated grid is uniform in the longitudinal direction and stretched in the vertical direction to have the centre point of the wall-adjacent cell at a height of 1 m.

The velocity profile is taken from the blind-test exercise (Richards et al., 2002), whereas the k profile is specified using both the relations proposed by Richards and Hoxey (1993) and the one obtained using the semi-empirical correlation by Brost and Wyngaard (1978). As for the wind-tunnel scale test case, a constant stress is applied to the upper boundary, while only the modified wall treatment (Section 2.2) is used to model the rough terrain properties, following the conclusions of the results obtained from the wind-tunnel scale simulations.

For both unperturbed ABL cases, numerical simulations are carried out using the FLUENT v6.3 steady, 2d, double precision, pressure based solver. The standard discretization scheme is applied to pressure, while second order schemes are adopted for momentum and turbulence quantities, and the SIMPLE algorithm is chosen for pressure–velocity coupling. The simulations are considered converged when the residuals level out, resulting in a decrease of at least six orders of magnitude.

3.3. Flow around a bluff-body

The flow around a single, rectangular building (CEDVAL A1-1, Leitl, 1998) is simulated using the new turbulence model and wall function formulation, to demonstrate the capabilities of the new approach.

The building (Fig. 3) has width 0.1 m, length 0.15 m, height H 0.125 m and 4 source elements on the leeward building side. In fact, the building configuration was used for studying the dispersion of a tracer gas from the source elements. In the present study, only the flow field is investigated; nevertheless, the mesh is conceived to allow modelling the dispersion in a further study.

The computational domain inlet boundary is set 1 m upstream of the building, where ABL profiles are measured in the wind tunnel, whereas the outlet boundary is located 4 m downstream of the building. As the model is symmetrical with respect to the plane $y=0$ m, only half of the domain is represented. The width and height of the domain are 0.65 and 1 m, respectively, corresponding to the wind-tunnel size. A structured mesh consisting of 1.7 million cells ($200\times114\times107$ elements) is applied. The height of the ground adjacent cell is 0.00075 m, which corresponds to one cell between the ground surface and the lower edge of the source elements. The new wall function formulation allows maintaining this resolution in the entire computational domain. Previous investigations (Gorlé et al., 2010) employed the standard rough wall formulation with a modification of the roughness constant C_s, following Blocken et al. (2007b). As a consequence, the computational grid had to be non-conformal, with coarser

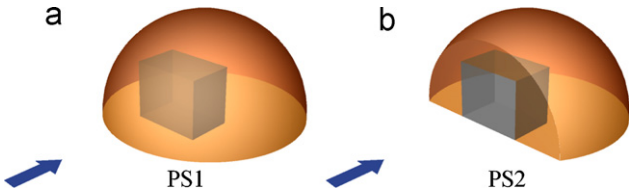

Fig. 4. Configurations PS1 (a) and PS2 (b) for the definition of the building influence area (BIA).

Table 2
Hit rate values for non-dimensional velocity and turbulent kinetic energy, varying the turbulence model settings.

	U/U_{ref}			
	Upstream	Side/Top	Downstream	All
Richards and Hoxey BCs	0.90	0.75	0.49	0.66
Gorlé et al. (2010)	0.87	0.81	0.59	0.71
PS1	0.89	0.78	0.56	0.70
PS2	0.90	0.79	0.58	0.71
	k/U_{ref}^2			
	Upstream	Side/Top	Downstream	All
Richards and Hoxey BCs	0.36	0.51	0.59	0.51
Gorlé et al. (2010)	0.54	0.31	0.49	0.47
PS1	0.54	0.40	0.54	0.52
PS2	0.58	0.54	0.62	0.59

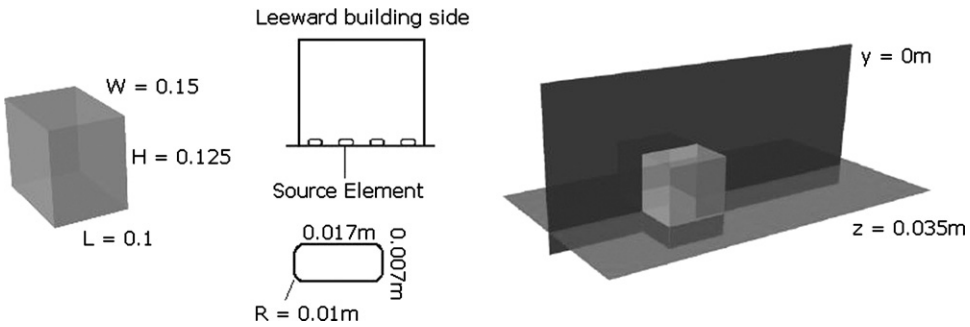

Fig. 3. Building geometry and location of measurement planes.

wall-adjacent cells in the far field, to allow the correct reproduction of the incoming ABL without exceeding the requirement $C_s \leq E$. Hence the test case is well suited to demonstrate the advantage of the new approach, which does not require the definition of a roughness constant (C_s) and allows preserving the same high near-wall resolution throughout the entire domain.

The presence of an obstacle immersed in the ABL flow has important modelling implications. The turbulence model formulation derived in the present paper (Section 2) is valid for an unperturbed ABL. As demonstrated by Gorlé et al. (2010), the application of turbulence model modifications derived for unperturbed ABL flows in regions of the flow affected by obstacles can negatively affect model predictions. It was shown that this problem can be alleviated by dividing the computational domain in two regions: a region unaffected by the building, where the modified turbulence model parameter C_μ and the source terms S_k and S_ε (Section 2) are applied, and a region influenced by the building, where the standard k–ε formulation is adopted. Beranek (1979) provided guidelines for the determination of the Building Influence Area (BIA) for wind flow around different building geometries. For the case under investigation, the BIA is set as a half sphere with radius $r = 1.6$ H and centre 0.16 H located downstream of the building. An additional test is also performed, to investigate the impact of the specified BIA on the results, by limiting the BIA to the region downstream of the building.

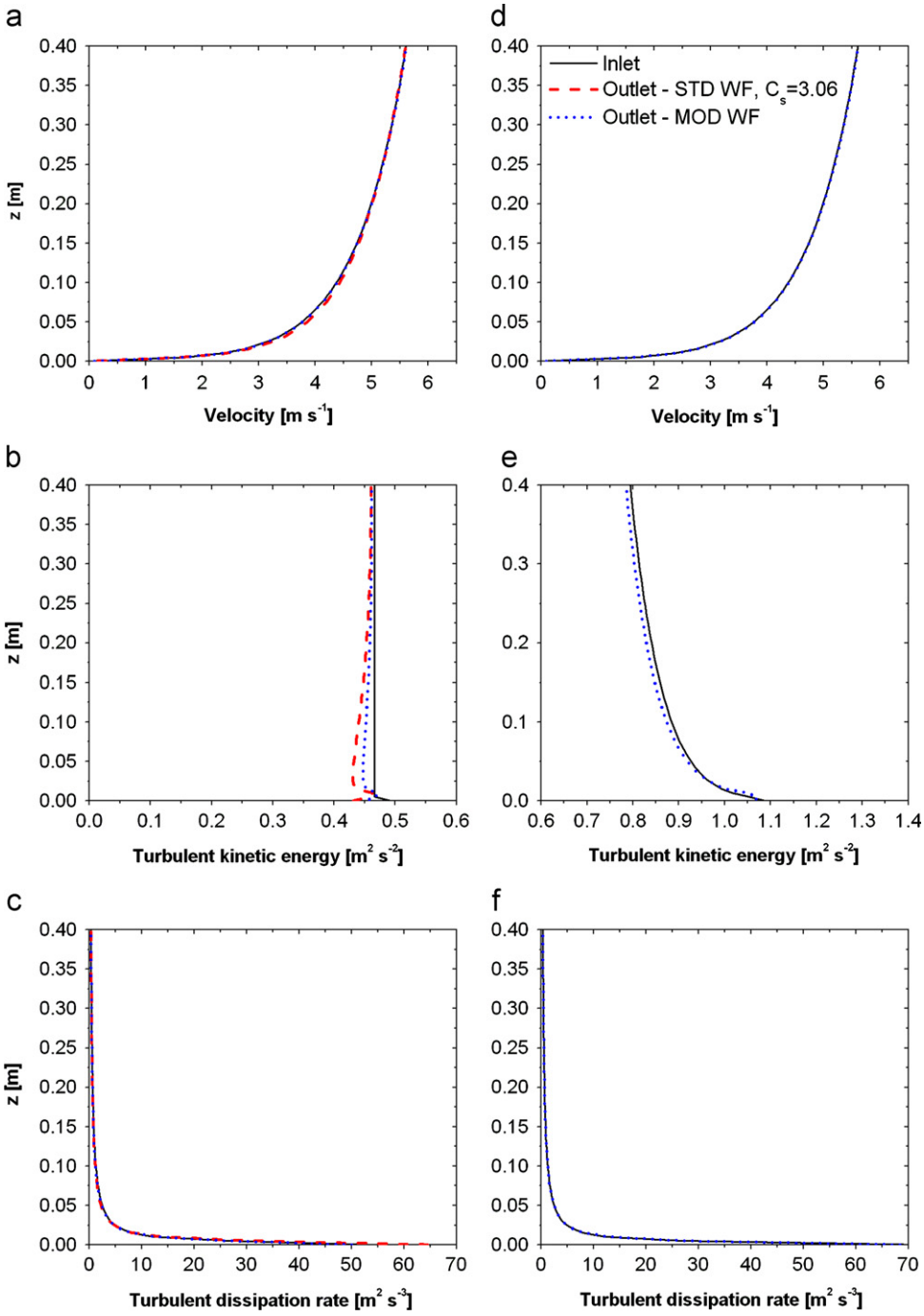

Fig. 5. Profiles of velocity, turbulent kinetic energy and turbulent dissipation rate at inlet and outlet section of the computational domain (Fig. 2a), obtained when applying inlet conditions given by Eqs. (5)–(7)(a–c) and Eqs. (5), (10) and (11)(d–f). STD WF = Standard Wall Function; MOD WF = Modified Wall Function.

The investigated configurations (Fig. 4) for the prescribed switch (PS) between the turbulence model formulations are referred to as PS1 and PS2. To ensure consistency of the model, a rough ground wall is applied in the regions where the ABL is unperturbed whereas a smooth ground wall is used in the BIA.

Results are compared to wind-tunnel test data of mean velocity and turbulent quantities, available at the measurement planes indicated in Fig. 3, namely the symmetry plane ($y=0$ m) and the horizontal plane $z=0.035$ m. The data are extracted and post-processed to obtain a 2D representation of the contours of time-averaged non-dimensional velocity component, u/U_{ref}, and non-dimensional turbulent kinetic energy, k/U_{ref}^2, where U_{ref} is the longitudinal reference velocity, where the reference velocity, $U_{ref}=5.81$ m/s, is the free stream velocity measured at $z=0.5$ m in the wind tunnel.

To quantify the agreement between measurements and numerical simulations, a hit rate q is defined for both velocity and turbulent kinetic energy as

$$q=\frac{1}{N}\sum_{i=1}^{N}\delta_i \tag{26}$$

where

$$\delta_i=\begin{cases}1 & \text{for } \left|\frac{V_{CFD}-V_{TEST}}{V_{TEST}}\right|\le 0.25 \text{ or } |V_{CFD}-V_{TEST}|\le W\\ 0 & \text{else}\end{cases} \tag{27}$$

The hit rate indicates the fraction of N measurement points at which the CFD results are within 25% of the measurement data or within the uncertainty interval, W, of the data (Franke et al., 2007). The value used for the uncertainty interval W is 0.012 for the non-dimensional velocity and $0.0316(k/U_{ref}^2)^{0.518}$ for the non-dimensional turbulence kinetic energy. The selected values affect the absolute value of the hit rate, but they are verified not to change the observed model performance trends. Both total hit rate for all measurement points and local hit rates for selected points (upstream, on the side, on top and downstream of the building) are presented in Table 2.

The Fluent v6.3 steady, 3d, double precision, pressure based solver is used for the bluff-body simulations. The standard discretization scheme is applied to pressure, while second order schemes are adopted for momentum and turbulence quantities, and the SIMPLE algorithm is chosen for pressure–velocity coupling. Numerical simulations are run until the residuals level out, resulting in a decrease of at least six orders of magnitude.

4. Results

4.1. Wind-tunnel unperturbed ABL

Fig. 5 shows the profiles of velocity, turbulent kinetic energy and dissipation rate at the inlet and outlet sections of the computational domain in Fig. 2a, for the inlet conditions specified by Eqs. (5)–(7) (Fig. 5a–c) and Eqs. (5), (10) and (11) (Fig. 5d–f).

For the case of a constant profile for turbulent kinetic energy, the results obtained with the standard wall function with a constant C_s defined via a UDF according to Eq. (20) are compared to those provided by the modified law of the wall. Results (Fig. 5a–c) indicate that the two approaches are consistent; however, the modified wall approach better preserves the homogeneity of velocity and turbulence throughout the domain. In particular, Fig. 5b and c confirms that the modification of C_s only affects the velocity profile, whereas the turbulent dissipation rate at the wall is overestimated, as a result of omitting the aerodynamic roughness in the denominator of Eq. (23). Consequently, the turbulent kinetic energy at the wall-adjacent cell is slightly underestimated.

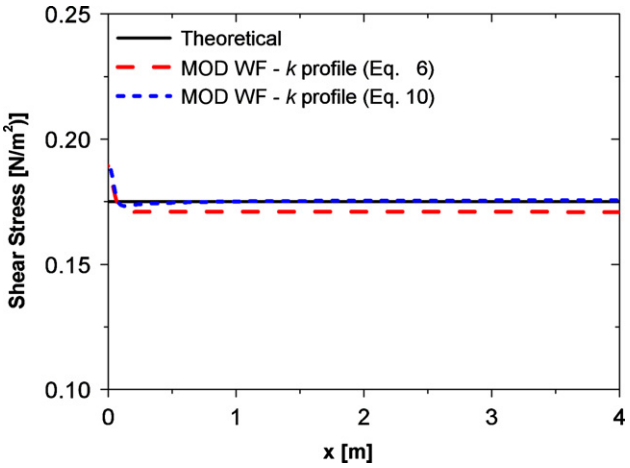

Fig. 6. Wall shear stress as a function of the axial coordinate for the wind-tunnel unperturbed ABL. MOD WF=Modified Wall Function.

Therefore, the formulation of the wall function alone already has a non-negligible impact on the simulation results, for what concerns the reproduction of the turbulent quantities.

For the case of a non-constant k profile, the comparison between the profiles of velocity, turbulent kinetic energy and dissipation rate at the inlet and outlet sections of the domain indicates that the proposed source terms (Section 2.1) and the implemented wall function ensure the desired longitudinal homogeneity. The highest differences are observed for the k profile, but they are below 4% in all cases.

Fig. 6 shows the evolution of the wall shear stress along the longitudinal coordinate for the two cases of constant and variable inlet k profiles. It can be remarked that the proposed approach produces a constant and realistic wall shear stress, after a short adaptation length. Moreover, for the case of a decreasing k profile (Eq. (10)), the predicted shear stress collapses onto the theoretical one, whereas small differences (below 6%) are observed for the constant k case.

4.2. Full-scale unperturbed ABL

Fig. 7 shows the profiles of velocity, turbulent kinetic energy and dissipation rate at the inlet and outlet sections of the computational domain in Fig. 2b, for the inlet conditions specified by Eqs. (5)–(7)(a–c) and Eqs. (5), (17) and (11)(d–f).

Similar to the wind-tunnel scale (Section 4.1), it can be concluded that the proposed modelling approach can be successfully applied to the numerical simulation of full scale, unperturbed ABL flows. As far as the longitudinal velocity component is concerned, maximum deviations of about 3% are observed for both sets of inlet conditions tested. The turbulent kinetic energy profile specified at the inlet section is also very well maintained throughout the computational domain: maximum differences of about 5% and 3% are observed when applying the Richards and Hoxey (1993) and Brost and Wyngaard (1978) boundary conditions for k. It is also interesting to observe that the semi-empirical correlations by Brost and Wyngaard (1978) result in a consistent level of turbulent kinetic energy, although slightly higher ($\sim$30%) than the one provided by Eq. (6) (Richards and Hoxey, 1993).

Finally, the wall shear stress along the longitudinal coordinate (Fig. 8) indicates that a constant and realistic shear stress is retrieved also for the full-scale ABL simulation. Moreover, analogously to the wind-tunnel case, the predicted shear stress matches the theoretical value for the case of a variable k profile (Eq. (10)) almost exactly.

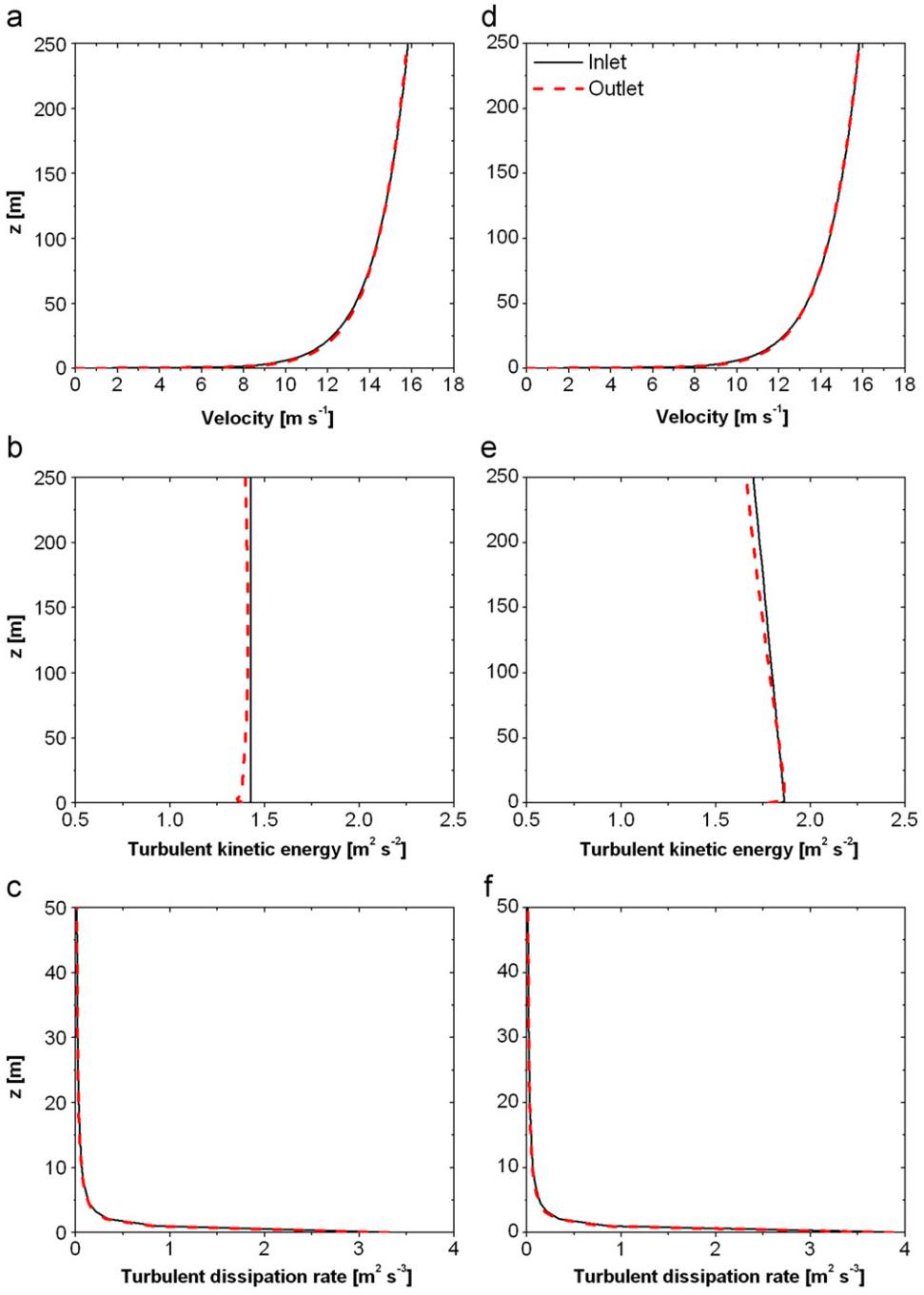

Fig. 7. Profiles of velocity, turbulent kinetic energy and turbulent dissipation rate at inlet and outlet section of the computational domain (Fig. 2b), obtained when applying inlet conditions given by Eqs. (5)–(7)(a–c) and Eqs. (5), (17) and (11)(d–f). Results obtained with the novel wall function formulation (Section 2.2).

4.3. *Flow around a bluff-body*

Table 2 presents the hit rates for the different model settings. In addition to the PS1 and PS2 results, the result presented by Gorlé et al. (2010) for settings similar to the present PS1 and the result obtained using the classic Richards and Hoxey (1993) boundary conditions with the standard k–ε model are included for reference. For the velocity, an improvement in the hit rate is obtained using any of the modified approaches as compared to the Richards and Hoxey (1993) boundary conditions. Moreover, we observe no major differences in the hit rate for u/U_{ref} between the PS1 or PS2 settings. For the turbulence kinetic energy, however, the PS2 setting produces a significant increase in the hit rate (59%) with respect to the PS1 settings (52%). An important improvement is also observed with respect to the reference case from Gorlé et al. (2010), which provides a hit rate of 47%, and the results obtained using the Richards and Hoxey (1993) boundary conditions (51%), in all regions of the flow field. Based on these results, it was decided to focus any further analysis on the PS1 and PS2 configurations.

Figs. 9 and 10 present the contour plots for the non-dimensional velocity and turbulent kinetic energy, respectively, at planes $y=0$ and $z=0.035$ m. The experimental measurements are compared to the results obtained with the PS1 and PS2 configurations.

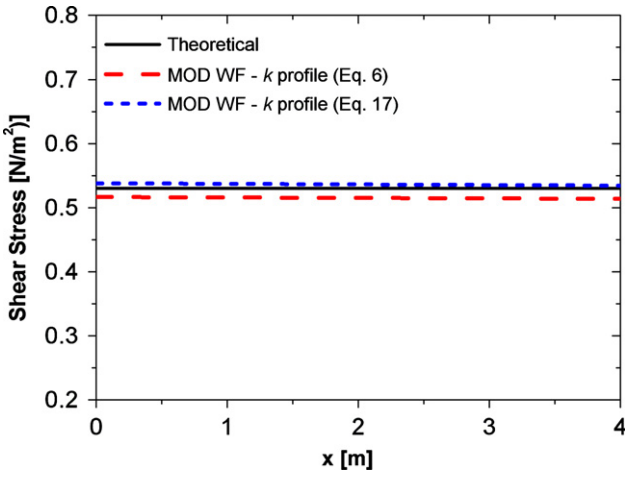

Fig. 8. Wall shear stress as a function of the axial coordinate for the full-scale unperturbed ABL. MOD WF=Modified Wall Function.

It can be observed that the main difference between the PS1 and PS2 settings is found in front of the building, with the PS2 setting resulting in a slightly better prediction of the upstream separation bubble and a smaller over-prediction of the turbulent kinetic energy. Both settings over-predict the size of the wake region by about 30% (~2.2 H versus ~1.7 H). However, a larger overestimation is obtained when applying the standard model and the Richards and Hoxey (1993) boundary conditions (~2.8 H versus ~1.7 H).

To allow a more quantitative comparison between experiments and numerical simulations, the calculated and measured non-dimensional vertical profiles of velocity, u, and turbulent kinetic energy, k, on the symmetry plane are shown in Figs. 11 and 12, respectively, for different locations upstream, over and downstream of the building. The different configurations (PS1 and PS2) used to prescribe the BIA are compared to the experimental measurements. It can be observed how the difference between the two configurations mainly affects the turbulent kinetic energy field (Fig. 12), in the region upstream of the building. In particular, the application of the ABL model at the axial location

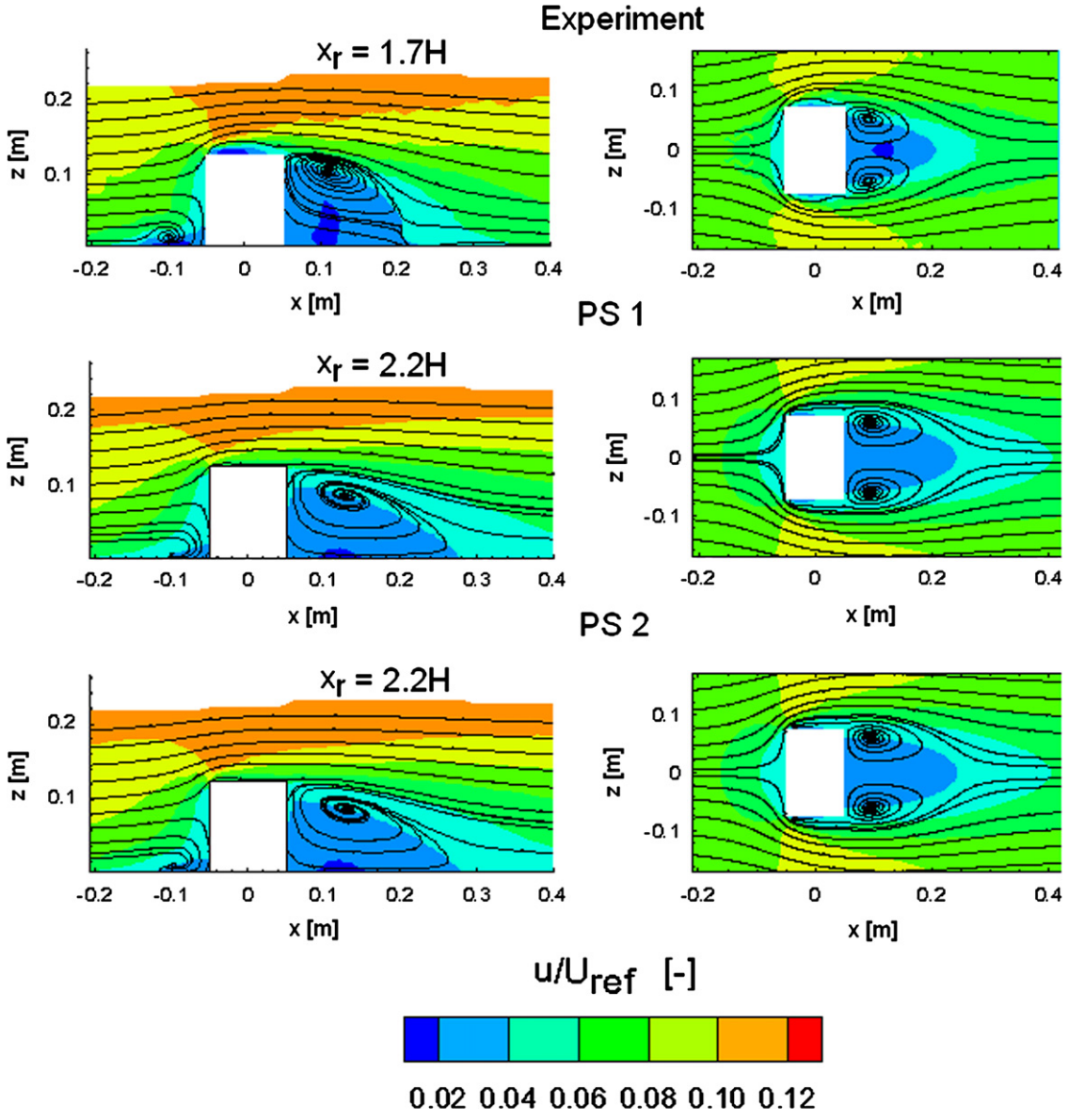

Fig. 9. Contour plots of non-dimensional velocity on the planes $y=0$ m (left) and $z=0.035$ m (right). Experimental measurements are compared to the results obtained applying the PS1 and PS2 model.

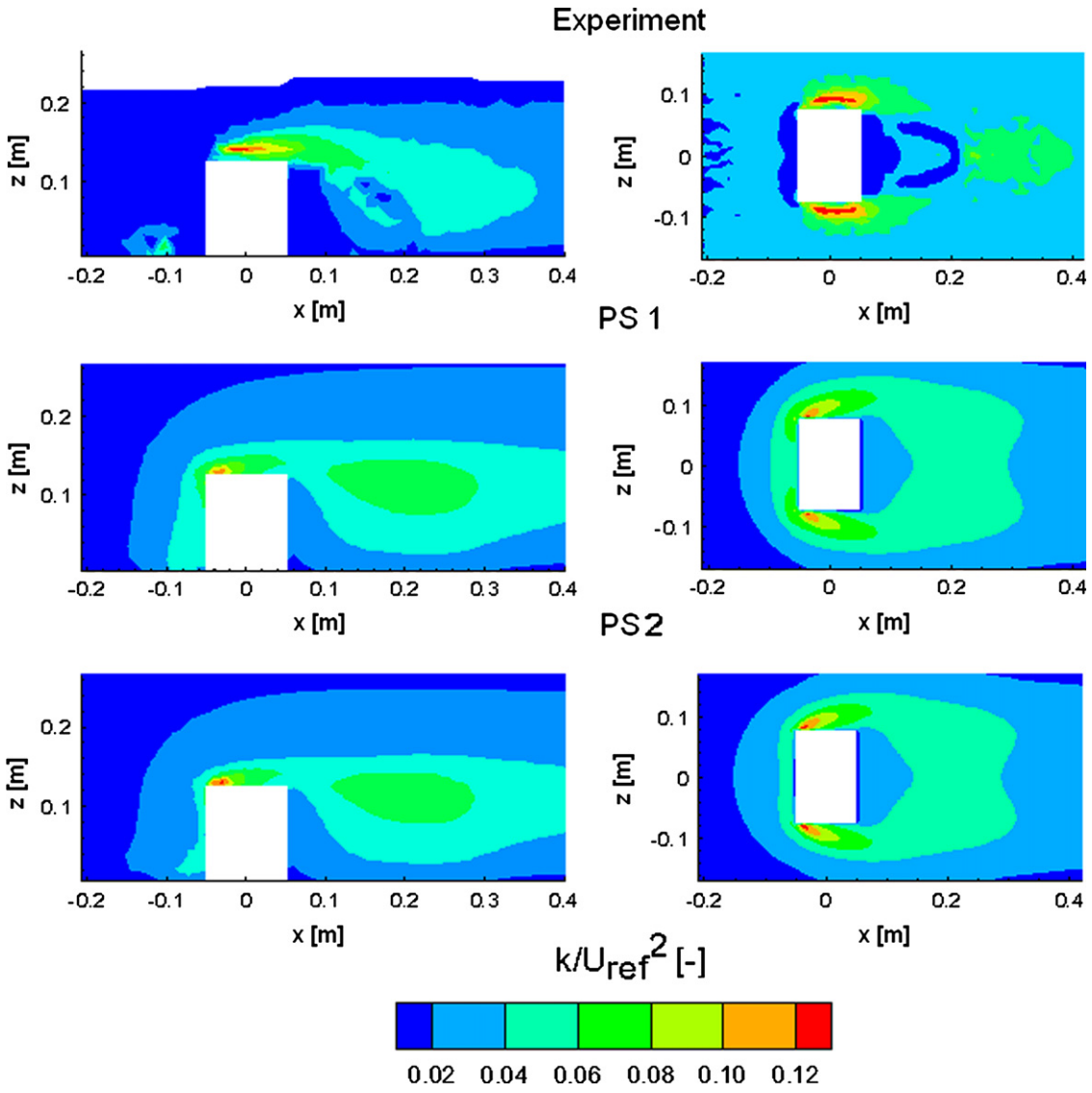

Fig. 10. Contour plots of non-dimensional turbulence kinetic energy on the planes $y=0$ m (left) and $z=0.035$ m (right). Experimental measurements are compared to the results obtained applying the PS1 and PS2 model.

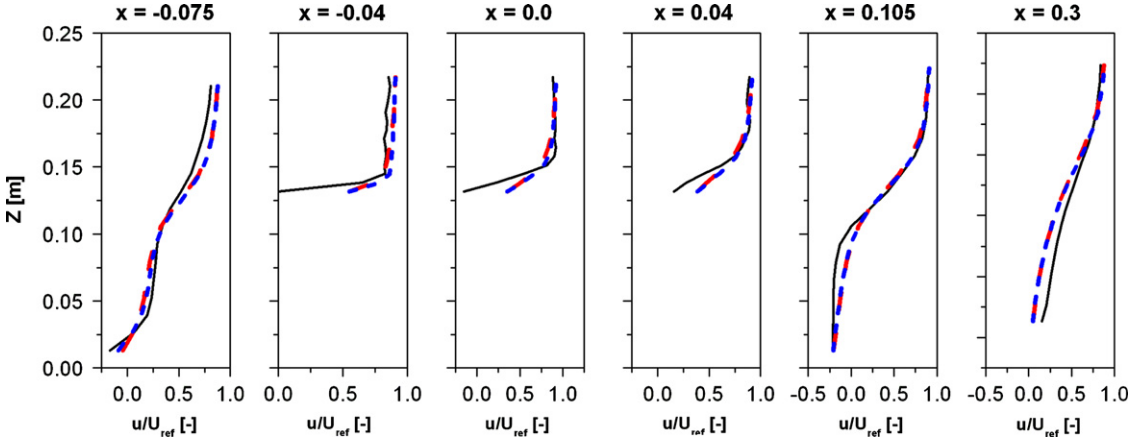

Fig. 11. Experimental and numerical profiles of non-dimensional velocity upstream, over and downstream of the obstacle. Solid line: experimental data. Dashes: PS1 configuration. Short dashes: PS2 configuration.

$x=-0.075$ m, allows significantly reducing the overestimation of turbulent kinetic energy. This effect remains at the first location on top of the building ($x=-0.04$ m). On the other hand, on the roof and further downstream ($x=0$ m and $x=0.04$ m) and behind the building ($x=0.105$ m and $x=0.3$ m), the two model predictions become comparable, almost collapsing onto a single line.

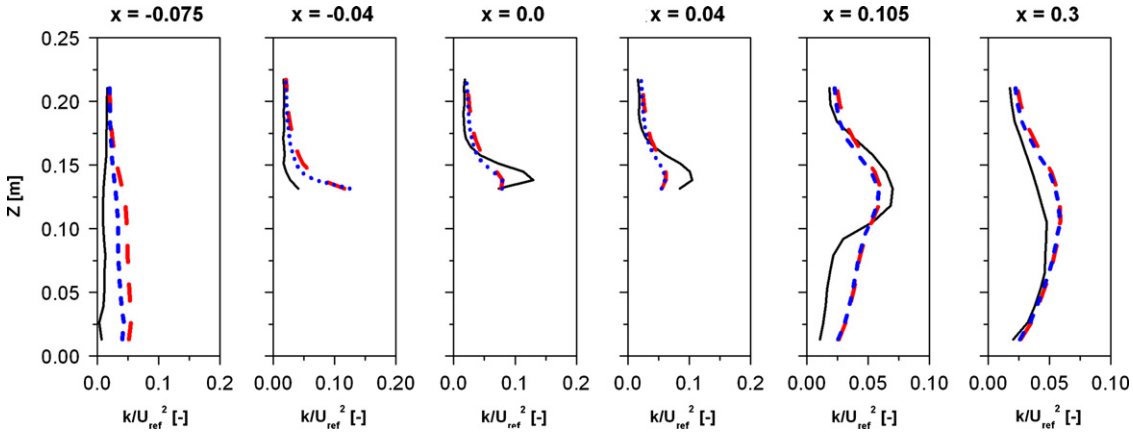

Fig. 12. Experimental and numerical profiles of non-dimensional turbulent kinetic energy upstream, over and downstream of the obstacle. Solid line: experimental data. Dashes: PS1 configuration. Short dashes: PS2 configuration.

The results presented in this Section confirm the need for advanced models, to allow a different turbulence model formulation in the flow region influenced by the building. The size of the BIA appears to have a non-negligible role in the results and in the accuracy of the predictions, suggesting that major improvements could be achieved by developing an automatic algorithm for the determination of the BIA. In particular, an approach based on the local departure from the undisturbed ABL conditions could provide a metric to automatically switch between different model formulations. Moreover, the use of the standard C_μ value in the BIA could not represent the best choice, and more complex formulations based on the relative importance of strain and vorticity are under investigation (Tsuchiya et al., 1997).

5. Conclusions

The present paper discusses a novel approach for the Reynolds-averaged Navier–Stokes modelling of neutral atmospheric boundary layer (ABL) flows using the standard k–ε turbulence model. A modification of the standard k–ε model consisting in the introduction of source terms for turbulent kinetic energy and dissipation rate is proposed, to allow the specification of arbitrary profiles of turbulent kinetic energy at the inlet boundary of the computational domain. Moreover a novel implementation of a general-purpose wall function for rough surfaces is presented. The rough wall function depends directly on the aerodynamic roughness, as prescribed by Richards and Hoxey (1993). Consequently, the boundary condition does not impose any limitation in terms of grid resolution and it offers more flexibility from the point of view of mesh generation and near-wall refinement.

Numerical simulations are performed for the case of an unperturbed neutral ABL, at both wind-tunnel and full scale, and for the flow around a bluff-body. Results indicate the capability of the proposed approach of ensuring the desired homogeneity of velocity and turbulent quantities throughout an empty computational domain.

The simulation of the flow around the bluff-body indicates how, in proximity of an obstacle, the homogeneous ABL formulation should be switched off, to allow a proper reproduction of the velocity and turbulence fields in the building influence area. The numerical simulations underline the relevance of the prescribed BIA shape on the accuracy of the predictions, suggesting the need for models able to automatically determine the shape of the BIA during the numerical simulation, without prescribing it *a priori*.

Acknowledgements

The authors would like to thank the group of Prof. Leitl at the University of Hamburg, for the availability of experimental data.

The second author's contribution to this work was supported by IWT Vlaanderen, the Institute for the Promotion of Innovation by Science and Technology in Flanders, through the SBO project NanoSoc, of the University of Antwerp, Department of Physics, EMAT.

References

Ansys Ltd., 2005. Ansys CFX-Solver, Release 10.0: Theory. Canonsburg.
Beranek, W., 1979. General rules for the determination of wind environment. In: Proceedings of the 5th International Conference on Wind Engineering, 225–234.
Bechmann, A., 2006. Large-eddy simulation of atmospheric flow over complex terrain, Ph.D. Thesis, Technical University of Denmark.
Blocken, B., Carmeliet, J., Stathopoulos, T., 2007a. CFD evaluation of wind speed conditions in passages between parallel buildings—effect of wall-function roughness modifications for the atmospheric boundary layer flow. Journal of Wind Engineering and Industrial Aerodynamics 95, 941–962.
Blocken, B., Stathopoulos, T., Carmeliet, J., 2007b. CFD simulation of the atmospheric boundary layer: wall function problems. Atmospheric Environment 41, 238–252.
Bottema, M., 1997. Turbulence closure model "constants" and the problems of "inactive" atmospheric turbulence. Journal of Wind Engineering and Industrial Aerodynamics 67–68, 897–908.
Brost, R.A., Wyngaard, J.C., 1978. A model study of the stably stratified planetary boundary layer. Journal of Atmospheric Sciences 35, 1427–1440.
CD-Adapco, User's Guide, 2008.
Cebeci, T., Bradshaw, P., 1977. Momentum Transfer in Boundary Layers. Hemisphere Publishing Corporation, New York.
Fluent, 2006. Fluent 6.3 User's Guide. Lebanon, New Hampshire.
Franke, J., Hellsten, A., Schlunzen, H., Carissimo, B. (Eds.), 2007. Best Practice Guideline for the CFD Simulation of Flows in the Urban Environment, COST Action 732.
Gorlé, C., van Beeck, J., Rambaud, P., Van Tendeloo, G., 2009. CFD modelling of small particle dispersion: the influence of the turbulence kinetic energy in the atmospheric boundary layer. Atmospheric Environment 43, 673–681.
Gorlé, C., van Beeck, J., Rambaud, P., 2010. Dispersion in the wake of a rectangular building: validation of two RANS modelling approaches. Boundary Layer Meteorology 137, 115–133.
Hargreaves, D., Wright, N., 2007. On the use of the k–ε model in commercial CFD software to model the neutral atmospheric boundary layer. Journal of Wind Engineering and Industrial Aerodynamics 95, 355–369.
Leitl, B., 1998. Cedval at Hamburg University. 〈http://www.mi.uni-hamburg.de/Introducti.433.0.html〉, accessed in January 2010.
Nikuradse, J., 1933. Stromungsgesetze in rauhen Rohren. Forschung Arb. Ing.-Wes. No. 361.
Norris, S.E., Richards P.J., 2010. Appropriate boundary conditions for computational wind engineering models revisited. In: Proceedings of the Fifth International Symposium on Computational Wind Engineering (CWE2010) Chapel Hill, North Carolina, USA May 23–27.

Parente, A., Benocci, C., 2010. On the RANS simulation of neutral ABL flows. In: Proceedings of the Fifth International Symposium on Computational Wind Engineering (CWE2010) Chapel Hill, North Carolina, USA May 23–27.

Pontiggia, M., Derudi, M., Rota, R., 2009. Hazardous gas dispersion: a CFD model accounting for atmospheric stability classes. Journal of Hazardous Materials 171 (1–3), 739–747.

Richards, P., Hoxey, R., 1993. Appropriate boundary conditions for computational wind engineering models using the k–ε turbulence model. Journal of Wind Engineering and Industrial Aerodynamics 46–47, 145–153.

Richards, P.J., Quinn, A.D., Parker, S., 2002. A 6 m cube in an atmospheric boundary-layer flow. Part 2. Computational studies. Wind Structures 5 (2–4), 177–192.

Riddle, A., Carruthers, D., Sharpe, A., McHugh, C., Stocker, J., 2004. Comparisons between FLUENT and ADMS for atmospheric dispersion modelling. Atmospheric Environment 38, 1029–1038.

Tsuchiya, M., Murakami, S., Mochida, A., Kondo, K., Ishida, Y., 1997. Development of a new k–ε model for flow and pressure fields around bluff body. Journal of Wind Engineering and Industrial Aerodynamics 67–68, 169–182.

Yang, Yi., Gu, M., Chen, S., Jin, X., 2009. New inflow boundary conditions for modeling the neutral equilibrium atmospheric boundary layer in computational wind engineering. Journal of Wind Engineering and Industrial Aerodynamics 97, 88–95.

Xie, Z., Voke, P.R., Hayden, P., Robins, A.G., 2004. Large-eddy simulation of turbulent flow over a rough surface. Boundary Layer Meteorology 111, 417–440.